Characterization of pack cemented Ni2Al3 coating exposed to KCl(s) induced corrosion at 600 °C

Dahl, Kristian Vinter; Slomian, A.; Lomholt, Trine Nybo; Kiamehr, Saeed; Grumsen, Flemming Bjerg; Montgomery, Melanie; Jonsson, T.

Published in:
Materials at High Temperatures

Link to article, DOI:
10.1080/09603409.2017.1392112

Publication date:
2018

Document Version
Peer reviewed version

Characterization of pack cemented Ni_2Al_3 coating exposed to KCl(s) induced corrosion at 600˚C

K. V. Dahl*[1], A. Slomian[2], T. N. Lomholt[1,3], S. Kiamehr[1], F. B. Grumsen[1], M. Montgomery[1] and T. Jonsson[2]

[1)] *Department of Mechanical Engineering, Technical University of Denmark, Produktionstorvet building 425, DK-2800 Kgs. Lyngby, Denmark*

[2)] *Environmental Inorganic Chemistry, Department of Chemistry and Chemical Engineering, Chalmers University of Technology, S-412 96, Göteborg, Sweden*

[3)] *Now at FORCE Technology, Park Alle 345, 2605 Brøndby, Denmark*

* kvd@mek.dtu.dk

Characterization of pack cemented Ni_2Al_3 coating exposed to KCl(s) induced corrosion at 600˚C

Oxidation of Ni_2Al_3 produced by pack aluminizing of pure nickel was studied with and without 0.10 mg cm^{-2} KCl(s) deposit in an environment containing 5% O_2, 40% H_2O and 55% N_2 at 600 °C for up to 168 h. Oxide microstructure and composition was investigated by SEM/EDX, BIB, TEM and GDOES. Oxidised Ni_2Al_3 shows minimal weight gain, while adding KCl results in a small weight loss consistent with evaporation of KCl. On the surface of samples exposed to the gas environment only, a 30nm oxide of Al oxide was present, but where KCl was present as deposit, 50-250 nm thick nodules form that are enriched in K, O and Al.

Keywords: Nickel aluminide; KCl, High temperature corrosion, 600˚C; Electron microscopy

Introduction

Fireside corrosion in boilers is accelerated when firing biomass compared to firing coal. This has the consequence that the maximum allowable outlet steam temperature is lowered significantly when firing biomass in order to keep corrosion rates at an acceptable level to have sufficient lifetime of critical components. The fireside environment is typically characterized by a combination of high levels of reactive alkali (NaCl and KCl), HCl and relatively low SO_2 concentrations [1].

Extensive research on the corrosiveness of potassium chloride towards low alloyed, stainless steels and FeCrAl alloys has been performed e.g. [2-7]. This literature shows that in addition to chlorine, the corrosiveness of KCl on chromia forming steels is caused by degradation of the protective oxide through formation of alkali chromates. Therefore, an opportunity to increase the lifetime of biomass fired boilers is to change the material, either by coatings or better bulk materials that are more resistant towards alkali induced corrosion.

The Al_2O_3 forming on alumina forming alloys and aluminides in oxidising environments occur in different modifications depending on exposure conditions, i.e. time, temperature and gas composition. At low temperatures or in early stages of oxidation, metastable oxides such as γ-Al_2O_3, δ-Al_2O_3 or θ-Al_2O_3 can form, while at higher temperature or after prolonged time the stable polymorph α-Al_2O_3 will form [8]. The presence of water vapour can influence the oxide formation and it has been shown that formation of metastable γ-Al_2O_3 is promoted on FeCrAl in the presence of 40% H_2O at 900˚C [9]. Brumm and Grabke saw formation of γ-Al_2O_3 on NiAl after up to 50 h exposure at 800˚C in 0.13 bar O_2+He [8]. Agüero et al. [10] exposed iron-aluminide slurry coatings on P92 steel to steam oxidation at 650˚C; after 24 h the coating had developed a thin protective χ-Al_2O_3 with smaller amounts of γ-Al_2O_3 and α-Al_2O_3, which slowly transformed fully into α-Al_2O_3 and finally mixed Fe-Al oxides, when the coating was depleted in aluminium.

Nickel aluminide has in several cases also been shown to have good resistance against KCl induced corrosion. *Li* et al. [11] reported excellent performance of NiAl (50/50 at%) exposed beneath KCl deposit in air for 48 hours at 650˚C, while Fe_xAl_y type model alloys experienced extensive corrosion attack. Similar behaviour was reported for exposure beneath a mixed surface deposit of NaCl-KCl in air for 48 hours at 670˚C [12]. Passive behaviour was found for a Ni_2Al_3 pack aluminized diffusion coating after exposure beneath a KCl deposit in static lab air for 168 hours at 600˚C. With the characterization methods used (SEM/EDX and XRD) it was not possible to find increased reactivity compared to a salt-free reference exposure [13]. After testing for 168 hours at 560˚C in a more complex atmosphere simulating flue gas from a straw-firing plant (6 vol % O_2, 12 vol % CO_2, 400 ppmv HCl, 60 ppmv SO_2, balance N_2 on dry basis; the dry gas being lead through a heated humidifier resulting in a final H_2O

content of 13.4 vol%) localized aluminium depletion was found for a Ni_2Al_3 diffusion coating [14]. However, the mechanism controlling the initial stages of corrosion in the presence of small amounts of KCl(s) has not been subjected to detailed microstructural studies.

The present work investigates the initial corrosion performance of Ni_2Al_3 made by pack aluminizing of pure Ni. The Ni_2Al_3 is exposed both with and without small additions of KCl in a laboratory setting in order to look for indications of reactivity with advanced characterization tools (TEM/EDX). The results from the microstructural investigation is linked to the exposure conditions and compared with the performance of other materials tested under the same well controlled settings.

Experimental procedure

Aluminising by pack cementation

Pack cementation of Ni-samples (99.99+% purity) was undertaken in a tube furnace with an argon protective atmosphere. The pack mixture consisted of 10 wt.% aluminium powder (99.9% purity, max particle size 60µm), 84 wt.% Al_2O_3-filler and 6 wt.% anhydrous $AlCl_3$. Powders for the pack were weighed and mixed thoroughly. The pack powder and samples were packed into Al_2O_3-containers that were then inserted in the tube furnace. The pack was heated to 650ºC using a heating rate of approximately 10ºC/min, held for 8 hours and then after the treatment cooled to room temperature inside the furnace in argon flow.

Samples were semicircular discs with a radius of 12.5 mm and a thickness of 2 mm. Prior to aluminising, the flat sample surfaces were ground on SiC paper with grit sizes #320, #500 and #1000 and then thoroughly cleaned in ethanol. After aluminising the flat sample surfaces were ground on SiC paper grit size #4000 and polished with 3

and 1 µm diamond suspension. Samples were weighed before and after exposure using a Sartorious R 160 P scale.

Corrosion testing

KCl was applied to the samples by spraying a saturated solution of KCl in a 20:80 mixture of water and ethanol (99,5%) while continuously drying the sample with heated air prior to exposure. The desired degree of KCl surface coverage was 0.10 mg/cm^2. All samples were exposed at 600˚C in an environment containing 5% O_2, 40% H_2O and 55% N_2 in an electrically heated tube furnace with a gas flow of 1000 mL/min. The samples were exposed for 1, 24 and 168 hours, both with and without KCl. Two test samples were included for each test condition. After exposure, the samples were allowed to air cool followed by weighing.

Characterization

Samples were examined in an FEI Quanta 200 FEG ESEM equipped with an Oxford Inca 300 EDX system for chemical analysis in high vacuum mode. X-ray diffraction was performed in a Siemens D5000 Powder Diffractometer. Transmission electron microscopy was performed using a JEOL 3000F FEG-TEM. FIB sections for TEM were produced using an FEI Quanta 200 3D SEM; gold was sputtered on to the surface to protect the corrosion products before FIB lift-out using a Polaron Thermo VG Scientific SC7620 sputter coater. Broad ion beam (BIB) sections were produced in a Leica BIB workstation. Glow discharge optical emission spectrocopy (GDOES) was performed using a Horiba GD-Profiler 2™.

Results

Pack cementation

The treatment led to formation of a Ni_2Al_3 layer as shown in Figure 1. The presence of Ni_2Al_3 was confirmed by XRD; not shown. A thin zone is present between the Ni_2Al_3 layer and the bulk nickel. Phases that may form according to the phase diagram are NiAl, Ni_5Al_3 and Ni_3Al. NiAl has the fastest growth kinetics of these three phases [15] and therefore the thin zone is expected to primarily consist of NiAl.

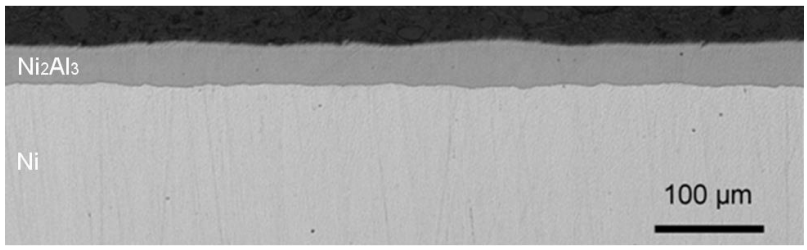

Figure 1. Reflected light optical image of the layer formed after aluminising at 650˚C for 8 hours.

Gravimetry

The corrosiveness of small amounts of KCl towards Ni_2Al_3 is illustrated in Figure 2 showing the mass gain in the gaseous environment (5% O_2 + 40% H_2O + N_2) with and without KCl(s) at 600 °C; similar exposures conducted for AISI 304L [3] and pure Ni [16] are included for comparison. Exposure of the Ni_2Al_3 coated samples reveals very small or negative mass gains, which indicate the formation of a protective oxide scale. The mass gain of the sample exposed for 168 hours without KCl corresponds to a calculated average oxide thickness in the nm range, based on Al_2O_3 formation. The scatter in mass gain is in addition very small. Exposures of the Ni_2Al_3 coated samples in the presence of KCl gives a mass loss approximately corresponding to the amount of deposited salt. KCl is known to evaporate under the given exposure conditions [3]. This

indicates that very little salt reacts with the Ni_2Al_3 phase and that a protective oxide forms in the presence of KCl, similar to the exposure without KCl. In comparison, the presence of KCl strongly accelerates the initial corrosion rate for AISI 304L stainless steel. In the absence of KCl after longer exposure times in the same gaseous atmosphere, a duplex oxide is formed due to evaporation of $CrO_2(OH)_2$ in the presence of water vapour [17]. Pure Ni both with and without KCl shows a similar behaviour as the stainless steel with KCl, i.e. similar increase in weight gain. Evaporation of KCl may explain the smaller mass gain of Ni exposed with KCl compared to exposures without KCl [16].

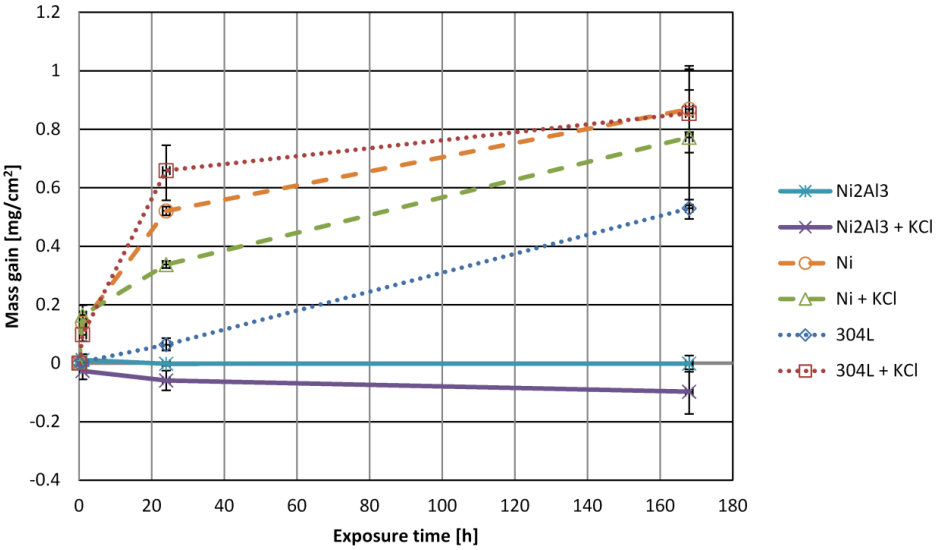

Figure 2. Mass gain of Ni_2Al_3 samples as well as 304L [3] and Ni [16] exposed with and without small amounts of KCl(s) in 5% O_2 + 40% H_2O + N_2 at 600 °C.

Characterization

Reference exposure

In the absence of KCl the Ni_2Al_3 coated samples showed very small mass gains. After one hour of exposure the sample surface was covered with a smooth oxide. Since the

appearance is very similar to the unexposed sample, this indicates that the scale is very thin, see Figure 3. The grain structure after short exposure times is visible due to contrast from channeling of electrons. The grain size varied over the surface. In some regions, the grain diameter was up to 20 µm while other regions had a grain size of about 5 µm. After 24 hours exposure, the oxide scale is still thin and transparent to the electron beam in the SEM. However, the surface appears to have a more undulating morphology, which makes the grain structure of the Ni_2Al_3 coating even more apparent. There is only a very small difference in contrast between grains in the BSE image indicating also small differences in oxide scale thickness on different grains. The samples exposed for 168 hours have an even more undulating surface morphology than the 24 hour samples. The Ni_2Al_3 grains are undulating while the grey scale in the BSE image again is similar indicating a similar thickness of the oxide scale on different grains. Grazing incidence XRD showed the presence of Ni_2Al_3, but it was not possible to identify the thin oxide scale.

A FIB/SEM lift out and subsequent TEM analysis revealed a 30 nm thick oxide layer rich in Al, see Figure 4. The TEM analysis confirmed the interpretation of the BSE images. The oxide scale was challenging to investigate in detail. Besides chemical composition, selected area diffraction (SAED) analysis and HRTEM imaging were employed in order to investigate if the oxide scale was crystalline. However, only indications of a crystalline scale could be observed, see HRTEM image in Figure 4B, and no conclusive diffraction pattern was identified. EDX from the middle of the layer yielded a composition of 42.3% Al, 1.3% Ni and 56.4% O in at%.

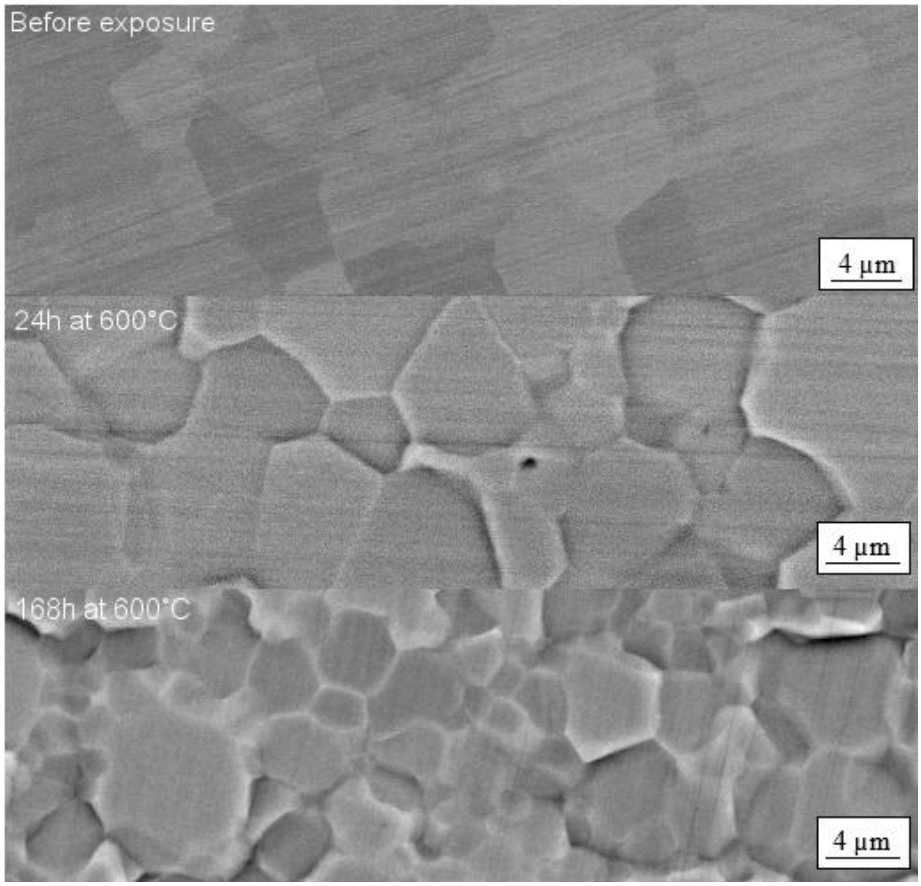

Figure 3. SEM/BSE images of sample surfaces after exposure for 0, 24 and 168 hours at 600˚C to 5% O_2 + 40% H_2O + N_2.

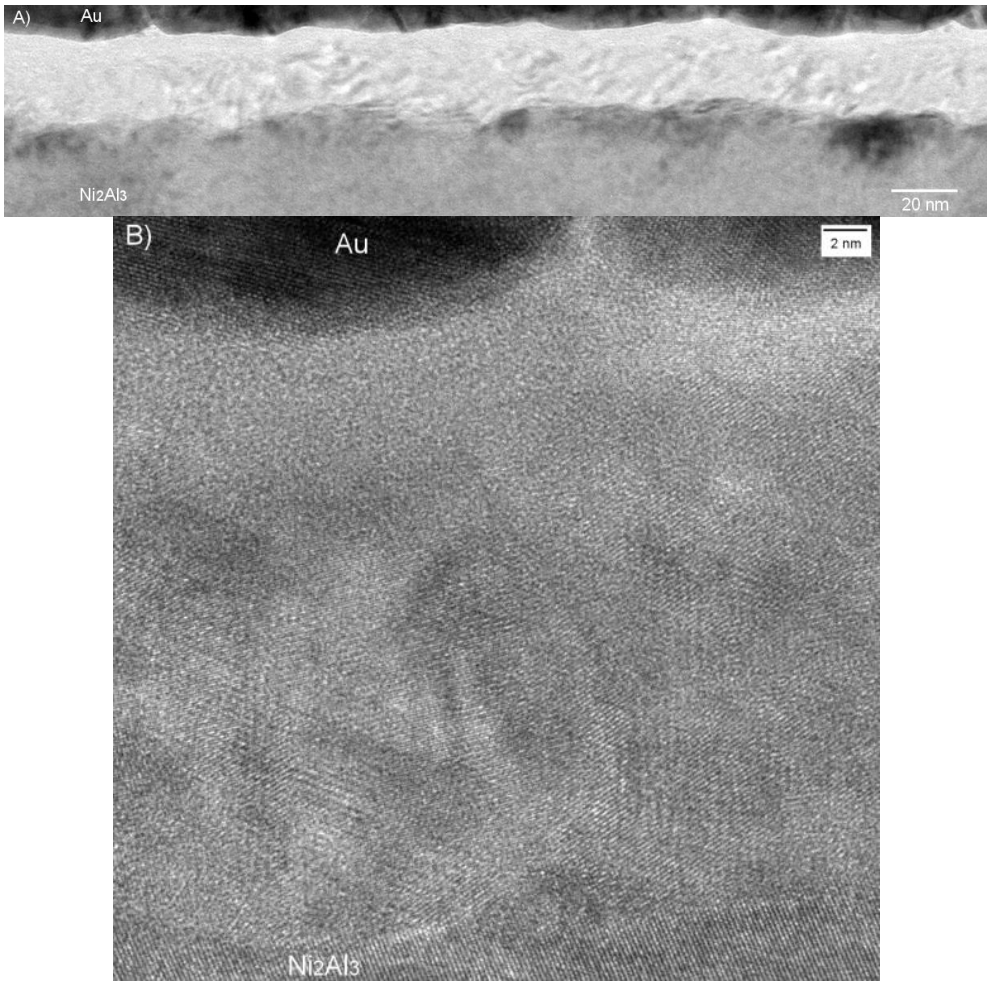

Figure 4. TEM images of oxide formed after exposure for 168 hours at 600˚C to 5% O_2 + 40% H_2O + N_2. A) Bright field overview, B) high resolution TEM (HRTEM).

Exposure with KCl

In the presence of KCl, all the Ni_2Al_3 coated samples showed a mass loss. The mass loss after 168h corresponds approximately to the evaporation of 0.1mg/cm^2 KCl, which was deposited on the surface. Oxidation with KCl(s) gave rise to morphology very similar to that observed on the samples exposed without KCl. No indications of an oxide rim could be observed in the vicinity of the KCl particles. At some locations, the final grinding after coating had not lead to a completely planar surface and here KCl particles could be found preferably in unpolished regions (valleys). However, no

changed morphology could be identified at such locations and the further characterization was carried out at locations with planar surface.

The low magnification BSE image in Figure 5A shows a similar morphology as that without KCl (cf. Figure 3) indicating a thin oxide scale all over the surface. After 24 hours exposure, most of the KCl had vanished due to evaporation but still some particles were left. Larger KCl particles had a tendency to lie at places with surface defects/unpolished regions, but this did not influence the oxide morphology of these regions. A high magnification SE image of the marked region in Figure 5A shows the vicinity of a remaining KCl particle, see Figure 5B. Small KCl particles could be observed but there was no indication of an oxide rim around these particles. No indication of spallation was observed. The oxide scale is still thin and transparent for the electron beam in the SEM. The sample exposed for 168 hours has very few KCl particles present. Similar to samples from the gaseous atmosphere only, the Ni_2Al_3 grains have an undulating surface morphology while the grey scale in the BSE image is similar indicating a similar thickness of the oxide scale on different grains, however, small-elongated nodules a few hundred nm in length are present over the surface, see Figure 6. This was not the case for the samples exposed without KCl.

GI-XRD again showed the presence of the Ni_2Al_3 but the phase of the very thin oxide scale could not be identified. KCl could only be detected on the sample exposed for one hour.

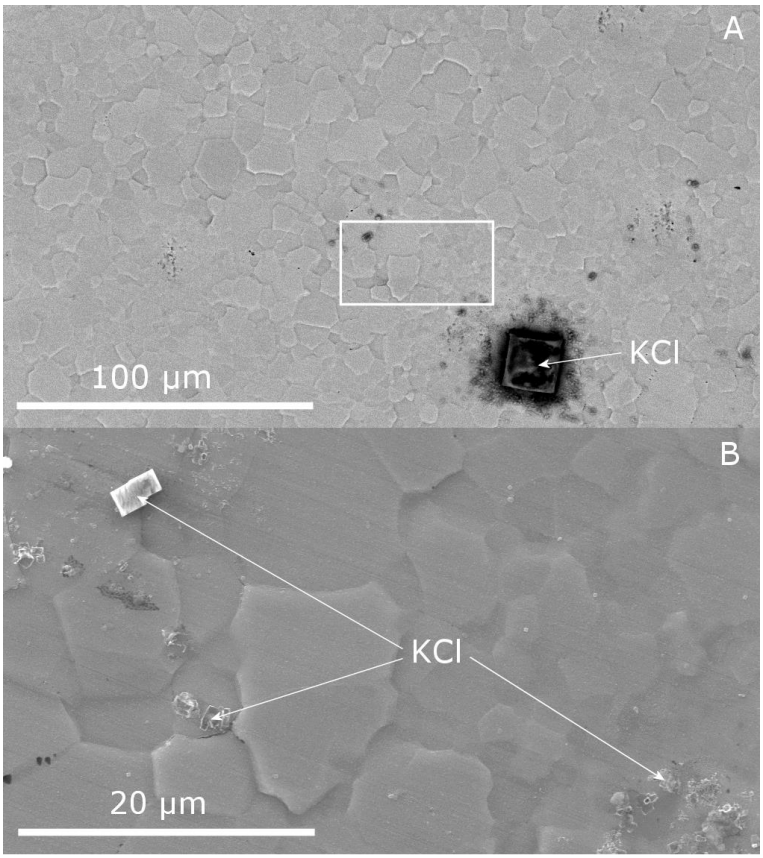

Figure 5. Ni_2Al_3 sample exposed to 5% O_2 + 40% H_2O + N_2 with KCl at 600˚C for 24h: A) SEM/BSE image. B) SEM/SE image of the region marked in image A.

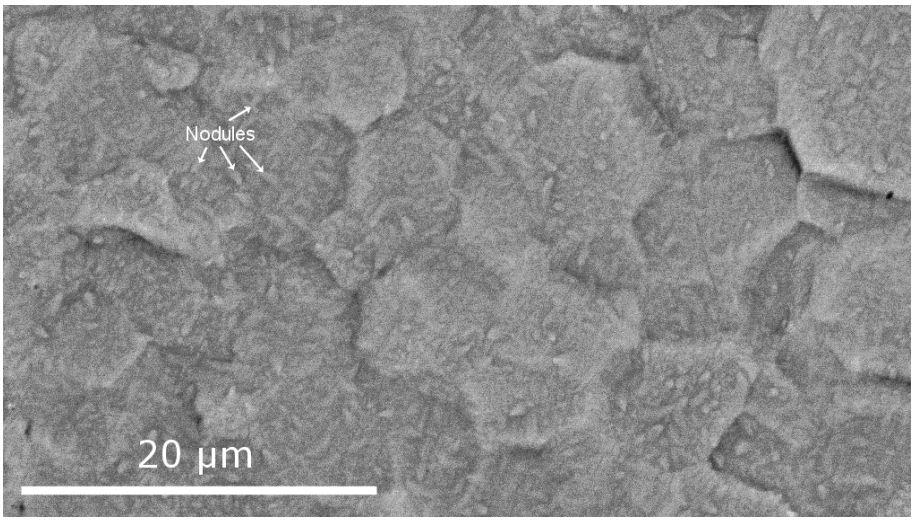

Figure 6. SEM/BSE image of Ni_2Al_3 coated sample exposed to 5% O_2 + 40% H_2O + N_2 with KCl at 600˚C for 168h.

A BIB cross-section was ion milled through the oxide scale and into the coating on a

Ni_2Al_3 coated sample exposed for 168h in the presence of KCl. In Figure 7, a SEM/BSE image depicts the resulting cross-section. The oxide is too thin to be identified in the cross-section, however, the different Ni-Al layers formed as a result of interdiffusion could be clearly observed. The Ni_2Al_3 layer is about 25 µm thick and has a grain size of about 15 µm. Beneath the Ni_2Al_3 layer, a 5 µm thick middle layer with composition corresponding to β-NiAl could be identified. The grain size of this layer is about 10 µm. The 10 µm thick bottom layer consists of 70 at.% Ni and 30 at.% Al and has a grain size of about 3 µm. There may be more layers present in between the observed layers but they are thin and difficult to resolve with the SEM/EDX. According to the Ni-Al phase diagram, both Ni_5Al_3 and Ni_3Al can be expected to form. None of the layers contain any voids in the ion-milled cross-section.

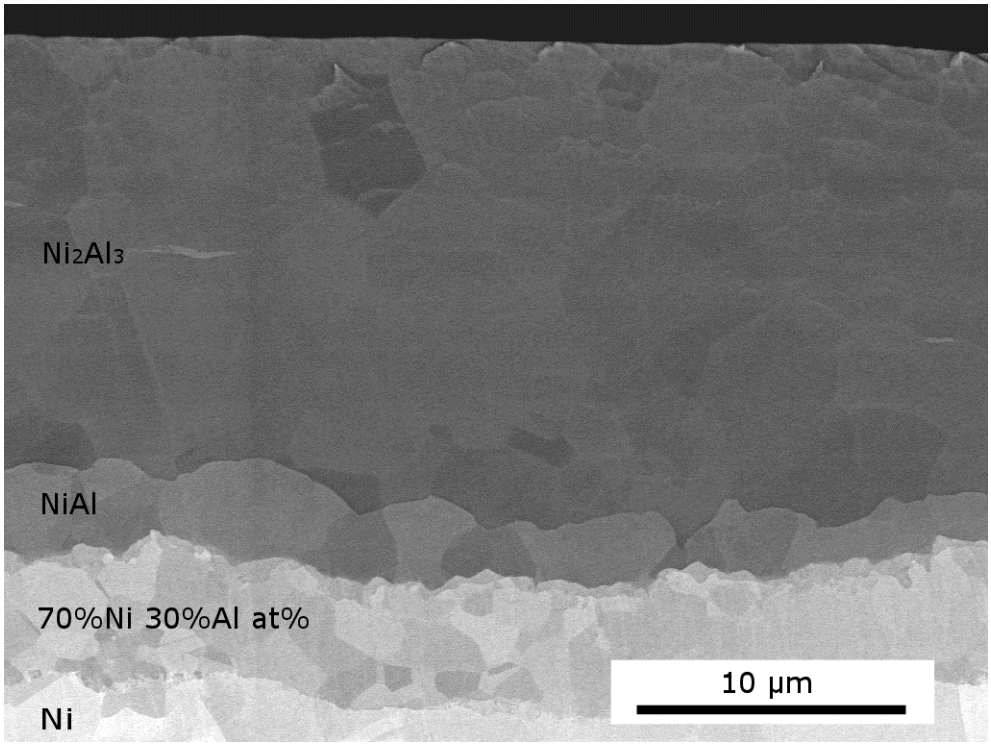

Figure 7. SEM/BSE image showing an ion milled cross-section of a Ni_2Al_3 coated sample exposed with KCl at 600 °C for 168h.

In order to investigate the thin protective scale on the surface after 168 hours, a TEM sample was prepared with the FIB/SEM workstation. Figure 8 shows a TEM bright field image of the oxide scale and subjacent Ni_2Al_3 coating. The oxide scale is 50nm-250nm in the cross-section, compared to the more uniform 30 nm thickness observed for the oxide on the sample exposed without KCl. The grain size of the Ni_2Al_3 coating is a few µm in this section and the undulating surface after 168 hours exposure could be confirmed. The nodules seen on the surface correspond to the small-elongated nodules seen in the SEM, cf. Figure 6.

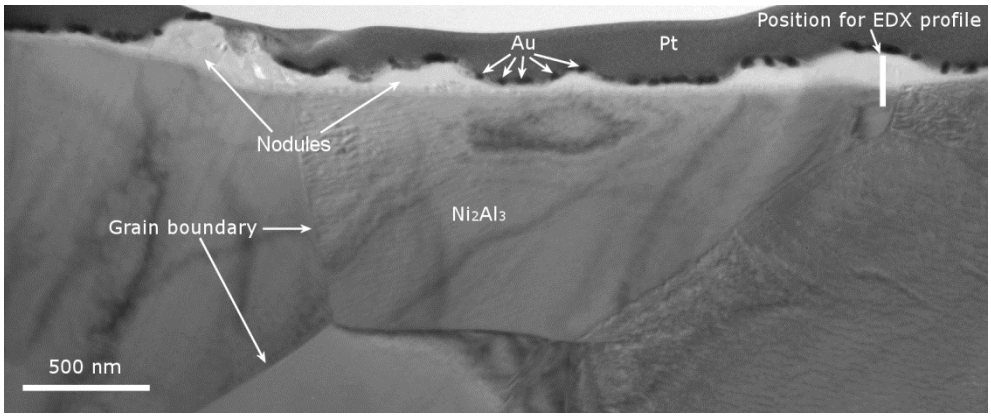

Figure 8. TEM/BF image showing the thin oxide scale in cross-section of a Ni_2Al_3 coated sample exposed to 5% O_2 + 40% H_2O + N_2 with KCl at 600 °C for 168h. The EDX profile shown in the next image was measured in the marked region

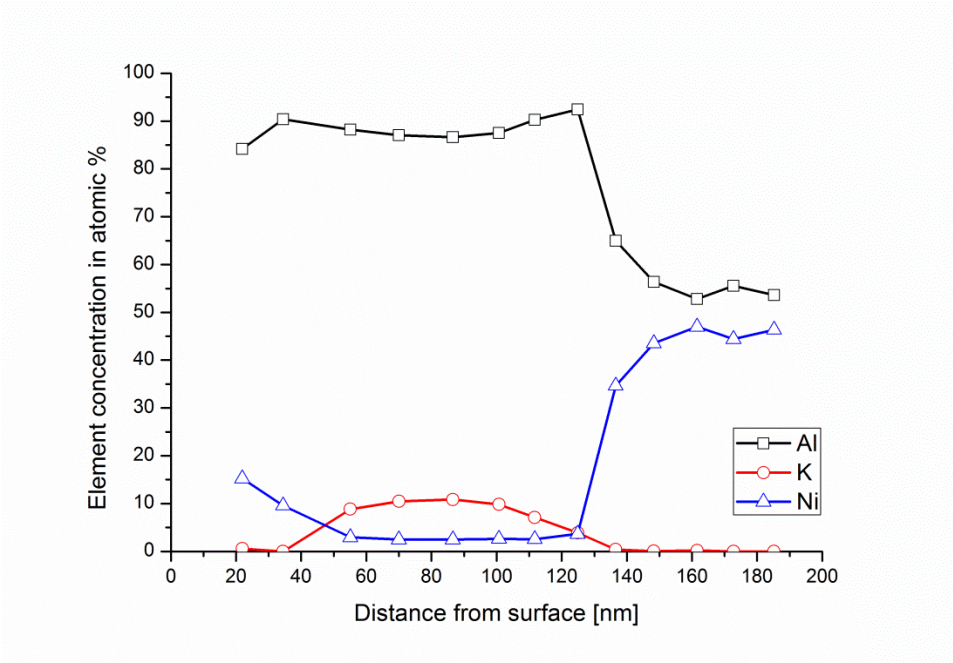

Figure 9. TEM/EDX results from the sample exposed to 5% O_2 + 40% H_2O + N_2 and KCl at 600 °C for 168h, from the position marked in Figure 8. Results are shown in cation at% in the line profile.

TEM/EDX on the electron transparent oxide scale resulted in hole formation in the thin oxide through electron-beam damage, but still revealed that the oxide scale contains O, Al, K and a small amount of Ni, see the results of EDX measurements in Figure 9. Only cation content is plotted in the EDX profiles. The oxygen content was measured to about 50 at.% in the oxide scale and no Cl was detected within the oxide. The signals from deposited gold and the copper grid were removed in the EDX quantification. The outermost part of the nodule is enriched in Ni, followed by a section enriched in K. Near the interface to the Ni_2Al_3, the K content drops. No measurable Al depletion in the bulk could be found with TEM/EDX. The decrease in K towards the interface to the bulk alloy, could indicate the formation of a more Al-rich oxide at the interface. This could be Al_2O_3 but it was not confirmed.

GDOES was performed on a sample exposed with KCl for 168 hours. The results shown in Figure 10 confirm the presence of K in the outer part of the scale. Since the surface is undulated and the nodules found on the surface vary in thickness the separation between different microstructure regions do not appear as sharp interfaces in the GDOES profiles. No attempt was made to try to convert the intensity measurements into quantitative data, since no suitable calibration sample was available; however, the intensity profiles are in agreement with the TEM/EDX data where quantification was performed. A weak intensity signal from Cl was also identified, but this could be due to residual KCl particles lying on the surface. The K peak immediately at the surface may be caused by such particles. After 10 s sputtering time, the oxide scale had been penetrated completely.

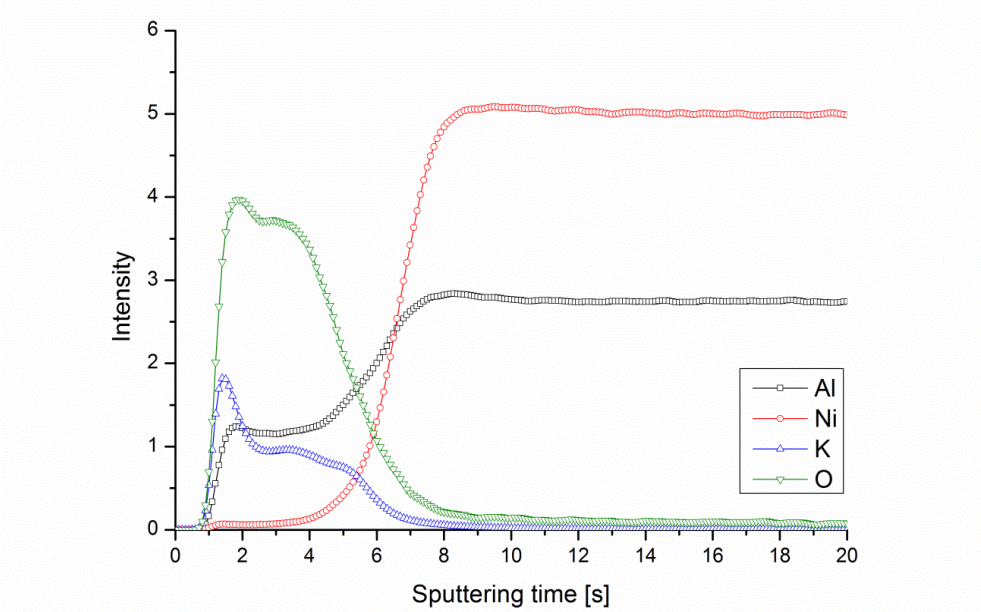

Figure 10. GDOES profiles measured on a sample exposed with KCl for 168h at 600˚C in 40% H_2O + 5% O_2 + N_2.

Discussion

Both the mass gain and the microstructure investigation confirm that the Ni_2Al_3 coating forms a protective aluminium rich oxide scale in 40% H_2O + 5% O_2 + N_2 after all

exposure times. The microstructural investigation indicate that a thin crystalline alumina scale has formed; it was not possible to identify the specific polymorph of Al_2O_3. Generally, γ-Al_2O_3 can often be found after (short) low temperature exposures [8], however also other possible modifications or mixtures are possible, e.g. χ-Al_2O_3 [10]. Further work is needed to identify the exact polymorph that formed on the Ni_2Al_3 in the present study. However, the behaviour of the scale is protective and the growth rate is in addition similar to that of protective chromium rich oxide scale formed on stainless steels at 600°C in O_2 [17].

Adding a small amount of KCl (0.10 mg cm^{-2}) to the surface of steel 304L generates a breakdown of the protective scale after a very short time span (1h) over large parts of the surface [3]. The breakdown mechanism is initiated by the formation of K_2CrO_4 depleting the Cr rich oxide of chromium. This results in a chromium poor oxide consisting of an outward growing iron rich oxide and an inward growing Cr,Fe,Ni oxide [18].

For pure Ni exposed to the same environment it was found that adding KCl did not result in an increase in corrosion rate, however a change in surface morphology was identified and small oxide crusts were observed in the vicinity of former KCl particles, which was proposed to be the result of an $NiCl_2$-KCl eutectic that forms at 514˚C [16].

For the Ni_2Al_3 coating investigated in the present work, there were no indications of crust formation around KCl particles. An $AlCl_3$-KCl eutectic can be found in the KCl-$AlCl_3$ phase diagram, see Figure 11. However, the amount of $AlCl_3$ is expected to be low on the surface because the vapour pressure of $AlCl_3$ is very high (P_{AlCl_3}=0.667 atm at 600˚C) (calculated by using the software FactSage 6.4 and

databases: Fact53, ELEM and BINS). Furthermore, $AlCl_3$ can be expected to be converted to oxides at very low oxygen partial pressures.

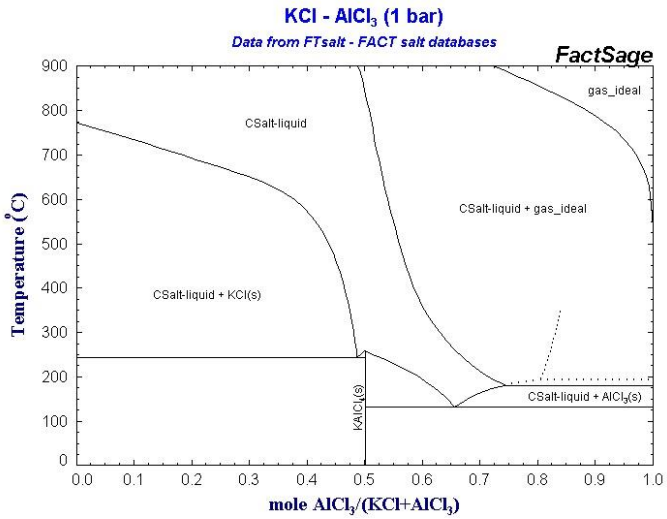

Figure 11. KCl-$AlCl_3$ phase diagram calculated with the software FactSage 6.4 and databases: Fact53, ELEM and BINS.

The morphology of the polished surface becomes undulating with longer exposure times for both exposures with and without KCl. A similar behaviour of surface rearrangement was observed at 1450 ºC in pure water vapour where evaporation was given as the cause [19]. The $Al(OH)_3$ is the most dominant vapour species but should be negligible at 600 ºC. Therefore the exact mechanism behind formation of the undulating surface needs further work to clarify. There are no indications that this influences the oxide scale on top of the Ni_2Al_3 grains or at the grain boundaries.

The microstructure investigation shows the formation of an aluminium rich oxide phase also in the presence of KCl. Based on the TEM-EDX findings a $K_xAl_yO_z$ reaction product formed in the surface nodules but it is slow growing and contains only smaller amounts of potassium.

In other work, no reactivity between KCl and a similar Ni_2Al_3 coating exposed under a KCl deposit at 600˚C for 168h in static lab air was found, even though it was

calculated to be thermodynamically possible to form e.g. KAl_9O_{14} during exposure with KCl (g) [13]. It was hypothesized that the characterization methods used (SEM/EDX and XRD) were not sufficient to reveal if reactivity had occurred on a nano-scale. In the present investigation, there is definite proof of reactivity between the coating and the KCl through the formation of K-containing nodules across the sample surface. It is suggested that the layer formed is KAl_9O_{14} as the K:Al atomic ratios measured in Figure 9 correspond to this compound and that it is probably formed from the presence of KCl(g). The outermost part of the nodule is enriched in Ni, followed by a section enriched in K. Brumm and Grabke [8] discuss that a possible mechanism for formation of Ni-rich outer oxides (NiO and $NiAl_2O_4$) on NiAl can be that they form during early stage oxidation and are subsequently undergrown by Al_2O_3 but remain stable at the oxide-gas interface. The mechanism in the present case could be similar. No chloride was observed at the oxide nodules where K was observed, or at the oxide metal interface, indicating the release of Cl possibly as HCl or small amounts of $AlCl_3$.

Despite the reaction of KCl with Al_2O_3, the general behaviour is protective up to 168 hours with only a small weight loss visible from gravimetry. This weight loss is consistent with evaporation of the added KCl, but it is difficult to completely rule out that a minor amount of $AlCl_3$ could have formed and contributed to the weight loss. For iron-rich aluminide coatings on P91 steel, selective aluminium removal was observed when exposed under a KCl deposit at 600 ˚C for 168h in static lab air. For Ni_2Al_3, local failures have also been observed for KCl induced corrosion in a more complex test-atmosphere [14] indicating that if the protective layer is penetrated, corrosion progresses fast, likely due to high volatility of $AlCl_3$. This may have implications for use in biomass boilers.

Conclusions

- Compared to 304L steel and pure Ni, the Ni_2Al_3 diffusion coating had very low corrosion rates in both exposures with and without KCl. For the exposure with KCl a weight loss was observed in the range expected from evaporation of KCl.
- For exposures with KCl, nodules up to 250 nm thick and rich in K, Al and O were identified across the exposed sample surface proving that there is reactivity.
- No chlorides were observed in the nodules or at the oxide/metal interface.

Acknowledgements

The project has been performed within the framework of the fifth stage of the material technology research programme (KME, in kind contribution from DONG Energy A/S). The work is in addition part of the Danish Strategic research centre, power Generation from REnewable Energy (GREEN) funded by the Danish Council for Strategic Research, grant no. 10-093956, EUDP grant 14-I, New Coatings for Biomass Firing and the Swedish High Temperature corrosion centre HTC.

References

[1] Nielsen HP, Frandsen FJ, Dam-Johansen K, Baxter LL. The implications of chlorine-associated corrosion on the operation of biomass-fired boilers. Progress in Energy and Combustion Science. 2000;26:283-298.

[2] Li YS, Niu Y, Spiegel M. High temperature interaction of Al/Si modified Fe-Cr alloys with KCl. Corros Sci. 2007;49(4):1799-1815.

[3] Jonsson T, Froitzheim J, Pettersson J, Svensson J-E, Johansson L-G, M Halvarsson M. The influence of KCl on the corrosion of an austenitic stainless

steel (304L) in oxidizing humid conditions at 600 ºC: A microstructural study. Oxid. Met. 2009;72:213-239.

[4] Karlsson S, Pettersson J, Johansson L-G, Svensson J-E. Alkali Induced High Temperature Corrosion of Stainless Steel: The Influence of NaCl, KCl and CaCl2. Oxid Met. 2012;78(1-2):83-102.

[5] Lehmusto J, Skrifvars B-J, Yrjas P, Hupa M. Comparison of potassium chloride and potassium carbonate with respect to their tendency to cause high temperature corrosion of stainless 304L steel. Fuel Process. Technol. 2013;105:98-105.

[6] Lehmusto J, Yrjas P, Skrifvars B-J, Hupa M. High temperature corrosion of superheater steels by KCl and K2CO3 under dry and wet conditions. Fuel Process. Technol. 2012;104:253-264.

[7] Israelsson N, Unocic KA, Hellström K, Jonsson T, Norell M, Svensson J-E, Johansson L-G. A Microstructural and Kinetic Investigation of the KCl-Induced Corrosion of an FeCrAl Alloy at 600 °C. Oxid. Met. 2015;84(1-2):105-127.

[8] Brumm MW, Grabke HJ. The oxidation behavior of NiAl-I. Phase transformations in the alumina scale during oxidation of NiAl and NiAl-Cr alloys. Corros Sci. 1992;33(11):1677-1690.

[9] Götlind H, Liu F, Svensson J-E, Halvarsson M, Johansson L-G. The Effect of Water Vapor on the Initial Stages of Oxidation of the FeCrAl Alloy Kanthal AF 900˚C. Oxid Met. 2007;67(5-6):251-266.

[10] Agüero A, Spiradek K, Höfinger S, Gutiérrez M, Muelas R. Microstructural evolution of slurry Fe aluminide coatings during high temperature steam oxidation. Mat. Sci. Forum. 2008;595-598: 251-259.

[11] Li YS, Spiegel M. Internal Oxidation of Fe-Al Alloys in a KCl-Air Atmosphere at 650˚C. Oxid. Met. 2004;61(3-4):303-321.

[12] Li YS, Spiegel M, Shimada S. Corrosion behavior of various model alloys with NaCl-KCl coating. Materials Chemistry and Physics. 2005;93:217-223.

[13] Kiamehr S, Lomholt TN, Dahl KV, Christiansen TL, Somers MAJ. Application of aluminium diffusion coatings to mitigate the KCl-induced high temperature corrosion. Materials and Corrosion. 2017;68(1):82-94.

[14] Wu D, Okoro SC, Dahl KV, Montgomery M, Pantleon K, Hald J. Laboratory Investigations of Ni-Al Coatings Exposed to Conditions Simulating Biomass Firing. In: Proceedings of the 9th International Symposium on High-Temperature Corrosion and Protection of Materials; 2016 May 15-20; Les Embiez Island, France

[15] Wang J, Wu DJ, Zhu CY, Xiang ZD. Low temperature pack aluminizing kinetics of nickel electroplated on creep resistant ferritic steel. Surface & Coatings Technology. 2013;236**:**135-141.

[16] Jonsson T, Slomian A, Lomholt TN, Kiamehr S, Dahl KV: Microstructural investigations of pure nickel exposed to KCl induced high temperature corrosion. Materials at high temperatures. 2015;32(1-2):44-49.

[17] Asteman H, Svensson J-E, Norell M, Johansson L-G. Influence of water vapor and flow rate on the high-temperature oxidation of 304L; Effect of chromium oxide hydroxide evaporation. Oxid. Met. 2000;54(1-2):11-26.

[18] Jonsson T, Karlsson S, Hooshyar H, Sattari M, Liske J, Svensson J-E, Johansson L-G. Oxidation After Breakdown of the Chromium-Rich Scale on Stainless Steels at High Temperature: Internal Oxidation. Oxid. Met. 2016;85(5-6):509-536.

[19] Opila EJ. Alumina Volatility in Water Vapor at Elevated Temperatures. J. Am. Ceram. Soc. 2004;87(9):1701-1705.

List of figure texts:

Figure 1. Reflected light optical image of the layer formed after aluminising at 650˚C for 8 hours.

Figure 2. Mass gain of Ni_2Al_3 samples as well as 304L [3] and Ni [16] exposed with and without small amounts of KCl(s) in 5% O_2 + 40% H_2O + N_2 at 600 °C.

Figure 3. SEM/BSE images of sample surfaces after exposure for 0, 24 and 168 hours at 600˚C to 5% O_2 + 40% H_2O + N_2.

Figure 4. TEM images of oxide formed after exposure for 168 hours at 600˚C to 5% O_2 + 40% H_2O + N_2. A) Bright field overview, B) high resolution TEM (HRTEM).

Figure 5. Ni_2Al_3 sample exposed to 5% O_2 + 40% H_2O + N_2 with KCl at 600˚C for 24h: A) SEM/BSE image. B) SEM/SE image of the region marked in image A.

Figure 6. SEM/BSE image of Ni_2Al_3 coated sample exposed to 5% O_2 + 40% H_2O + N_2 with KCl at 600˚C for 168h.

Figure 7. SEM/BSE image showing an ion milled cross-section of a Ni_2Al_3 coated sample exposed with KCl at 600 °C for 168h.

Figure 8. TEM/BF image showing the thin oxide scale in cross-section of a Ni_2Al_3 coated sample exposed to 5% O_2 + 40% H_2O + N_2 with KCl at 600 °C for 168h. The EDX profile shown in the next image was measured in the marked region

Figure 9. TEM/EDX results from the sample exposed to 5% O_2 + 40% H_2O + N_2 and KCl at 600 °C for 168h, from the position marked in Figure 8. Results are shown in cation at% in the line profile.

Figure 10. GDOES profiles measured on a sample exposed with KCl for 168h at 600˚C in 40% H_2O + 5% O_2 + N_2.

Figure 11. KCl-$AlCl_3$ phase diagram calculated with the software FactSage 6.4 and databases: Fact53, ELEM and BINS.